Research Square

Preprints are preliminary reports that have not undergone peer review.
They should not be considered conclusive, used to inform clinical practice,
or referenced by the media as validated information.

PSMA- and SSTR-targeted imaging and tissue characteristics in woodchuck hepatocellular carcinoma: an exploratory descriptive study

Hoda Poorbagher
University of Saskatchewan Western College of Veterinary Medicine
Monique Mayer
monique.mayer@usask.ca

University of Saskatchewan Western College of Veterinary Medicine https://orcid.org/0000-0003-3414-3918
Sally L. Sukut
University of Saskatchewan Western College of Veterinary Medicine
Ekaterina Dadachova
University of Saskatchewan College of Pharmacy and Nutrition
Humphrey Fonge
University of Saskatchewan College of Medicine
Sheldon Wiebe
University of Saskatchewan College of Medicine
Bruce K. Wobeser
University of Saskatchewan Western College of Veterinary Medicine
Matthew Hutcheson
University of Saskatchewan Western College of Veterinary Medicine
Vijayananda Kundapur
University of Saskatchewan College of Medicine
Alireza Doroudi
University of Saskatchewan College of Medicine
Kevin J. H. Allen
University of Saskatchewan College of Pharmacy and Nutrition
Carla S. Coffin
University of Calgary Cumming School of Medicine

Research Article

Keywords: Hepatocellular carcinoma, Woodchuck, Prostate-specific membrane antigen, Somatostatin receptors, PET/CT, Radiotheranostics, Animal model

Posted Date: November 11th, 2026

DOI: https://doi.org/10.21203/rs.3.rs-11447296/v1

License: This work is licensed under a Creative Commons Attribution 4.0 International License.
Read Full License

PSMA- and SSTR-targeted imaging and tissue characteristics in woodchuck hepatocellular carcinoma: an exploratory descriptive study

Hoda Poorbagher[1], Monique N. Mayer[1*], Sally L. Sukut[1], Ekaterina Dadachova[2], Humphrey Fonge[3], Sheldon Wiebe[3], Bruce K. Wobeser[4], Matthew Hutcheson[5], Vijayananda Kundapur[6], Alireza Doroudi[3], Kevin J. H. Allen[2], Carla S. Coffin[7]

[1] Department of Small Animal Clinical Sciences, Western College of Veterinary Medicine, University of Saskatchewan, Saskatoon, Saskatchewan, Canada.

[2] College of Pharmacy and Nutrition, University of Saskatchewan, Saskatoon, Saskatchewan, Canada.

[3] Department of Medical Imaging, College of Medicine, University of Saskatchewan, Saskatoon, Saskatchewan, Canada.

[4] Department of Veterinary Pathology, Western College of Veterinary Medicine, University of Saskatchewan, Saskatoon, Saskatchewan, Canada.

[5] Western College of Veterinary Medicine, University of Saskatchewan, Saskatoon, Saskatchewan, Canada.

[6] College of Medicine, University of Saskatchewan, Saskatoon, Saskatchewan, Canada.

[7] Department of Medicine, Gastroenterology, Cumming School of Medicine, University of Calgary, Viral Hepatitis Clinic, Alberta Health Services, Calgary, Alberta, Canada.

Present address (H. Fonge): Faculty of Pharmacy, Université Laval, Québec City, Québec, Canada; Centre de recherche du CHU de Québec–Université Laval, Québec City, Québec, Canada.

Present address (A. Doroudi): Centre de recherche du CHU de Québec–Université Laval, Québec City, Québec, Canada.

Correspondence: Monique N. Mayer, Department of Small Animal Clinical Sciences, Western College of Veterinary Medicine, University of Saskatchewan, 52 Campus Drive, Saskatoon, Saskatchewan S7N 5B4, Canada. Email: monique.mayer@usask.ca

Keywords: Hepatocellular carcinoma; Woodchuck; Prostate-specific membrane antigen; Somatostatin receptors; PET/CT; Radiotheranostics; Animal model

Abstract

Background: The use of prostate-specific membrane antigen (PSMA)- and somatostatin receptor (SSTR)-targeted radiotheranostics for hepatocellular carcinoma (HCC) requires preclinical models that reproduce the features of spontaneous tumors. Woodchucks chronically infected with woodchuck hepatitis virus (WHV) develop hepatic tumors that closely resemble hepatitis B virus-induced human HCC. We further characterized PSMA-targeted imaging and normal-tissue expression, including the salivary glands, and evaluated SSTR2/5 expression and [^{68}Ga]Ga-DOTATOC uptake. We also explored the feasibility and short-term tolerability of a single [^{177}Lu]Lu-PSMA-617 administration.

Results: Twelve tumor-bearing woodchucks underwent PET/CT imaging with [^{68}Ga]Ga-PSMA-11 or [^{68}Ga]Ga-DOTATOC (six animals each), with tissue expression assessed by quantitative reverse transcription polymerase chain reaction and immunohistochemistry. PSMA transcripts were detected in tumors, liver and salivary glands, and PSMA staining was present in tumor-associated microvessels and normal tissues. [^{68}Ga]Ga-PSMA-11 uptake varied within and between tumors, with a median tumor maximum standardized uptake value of 3.3 and tumor-to-liver ratio of 1.9. Uptake was also observed in salivary glands and other normal organs. Although SSTR2/5 transcripts and cytoplasmic staining were detected in tumors, only one of six animals showed strong [^{68}Ga]Ga-DOTATOC tumor uptake relative to liver. HCC was confirmed in all animals at necropsy. Tumors showed heterogeneous contrast enhancement, fibrosis and necrosis, and hepatic lymph node metastases were present in 6 of 10 animals in which lymph nodes were sampled. A single [^{177}Lu]Lu-PSMA-617 administration and serial follow-up were feasible in three animals; no changes in appetite or activity were observed.

Conclusions: SSTR-targeted imaging and normal-tissue characterization add to previous PSMA imaging findings in woodchuck HCC. The observed variation in tumor histopathology, target expression and radiopharmaceutical uptake supports further use of this model to study molecular imaging and radiopharmaceutical delivery in spontaneous HCC.

Background

Hepatocellular carcinoma (HCC) accounts for 75 to 85% of primary liver malignancies and is a leading contributor to cancer-related morbidity and mortality.[1-3] HCC is often asymptomatic in the early stages, with more than 80% of patients diagnosed with advanced-stage disease unamenable to current local therapies; the 5-year relative survival for patients with liver cancer is only 18%.[4] There is an urgent need for improved therapeutic options for these patients.

Radiotheranostics is an emerging modality that combines molecular imaging with targeted radionuclide therapy, offering the potential for improved clinical outcomes in patients with HCC. Small molecules, peptides, or antibodies directed at cell-specific epitopes are radiolabelled with gamma- or positron-emitting radionuclides for single-photon emission computed tomography (SPECT) or positron emission tomography (PET) imaging to assess the expression and accessibility of the target.[5] The same or similar targeting agent is then conjugated to an alpha- or beta-emitting radionuclide to achieve localized tumor cell killing. To date, two radiotheranostic agents have received regulatory approval: one targeting prostate-specific membrane antigen (PSMA) for metastatic prostate cancer ([^{177}Lu]Lu-PSMA-617), and another targeting somatostatin receptors (SSTRs) for the treatment of gastroenteropancreatic neuroendocrine tumors ([^{177}Lu]Lu-DOTATATE).[5,6]

Given the clinical success of radiotheranostics for prostate and gastroenteropancreatic neuroendocrine cancer, the expression of PSMA and SSTRs has been investigated in other malignancies, including HCC. Immunohistochemical (IHC) analysis revealed positive PSMA staining in 87% (245/282) of human HCC samples, with expression localized to the tumor-associated neovasculature in 83% (235/282) of samples.[7-10] Consistent with the high prevalence of PSMA expression detected by IHC, [^{68}Ga]Ga-PSMA-11 uptake was observed on PET imaging in 95% (76/80) of patients with newly diagnosed and recurrent primary HCC cases.[8-18] More recent prospective studies using PSMA-targeted PET/magnetic resonance imaging and PET/computed tomography (CT) have further demonstrated tracer uptake in HCC.[19-21] SSTRs also have potential for radiotheranostic applications. SSTR2, the receptor subtype for which [^{177}Lu]Lu-DOTATATE exhibits the highest affinity[22], was detected in 53% (136/259) of HCC samples by IHC.[23-27] Incidental findings of HCC uptake on SSTR-targeted PET imaging have been described in some patients.[28-30] These findings support the ongoing investigation of PSMA and SSTRs as promising targets for HCC radiotheranostics.

Clinically relevant preclinical models are essential for evaluating the therapeutic potential of PSMA- and SSTR-targeted radiotheranostics. While two-dimensional cell culture systems are widely used in early development, they lack cellular heterogeneity and the extracellular matrix components that influence tumor cell behavior and response to therapy.[31] Three-dimensional spheroid models provide cellular heterogeneity but do not fully reproduce the extracellular matrix, limiting their translational relevance.[31] *In vivo* murine models overcome some of these limitations, enabling assessment of tracer biodistribution, target and off-target uptake, and therapeutic efficacy. The most widely used *in vivo* models for theranostic research are immunocompromised mice bearing human tumor xenografts[32-34];

however, the absence of an intact immune system compromises the tumor microenvironment, which is composed of support cells embedded in the extracellular matrix. The tumor microenvironment can constitute over 50% of the tumor mass and plays a crucial role in response to therapy.[35] To address this limitation, syngeneic mouse models (immunocompetent mice implanted with murine cancer cells) and humanized mice (modified to possess a human-like immune system) are occasionally used but still fail to fully replicate key features of the tumor microenvironment of a spontaneous, orthotopic tumor, which include hypoxia, acidic pH, elevated interstitial pressure, dense extracellular matrix, and increased metabolic activity.[31] These factors, as well as variable perfusion and off-target tissue toxicity, are barriers to tumor penetration by radiotheranostic agents and to uniform distribution of agents within the tumor.[36,37] Physiologically relevant models that accurately mirror these barriers are essential for advancing radiotheranostics toward clinical translation. Specific to investigations of PSMA neovasculature targeting in solid tumors and dose-limiting toxicity, an additional limitation of mouse models is the reported absence of PSMA expression in neovasculature in some xenograft models and low expression in salivary glands.[38-40]

Eastern North American woodchucks (*Marmota monax*) chronically infected with woodchuck hepatitis virus (WHV) reliably develop virus-induced hepatic tumors that closely resemble hepatitis B virus-induced human HCC in patients with chronic hepatitis B.[41] Neoplastic transformation occurs through direct hepadnaviral integration into hepatocyte deoxyribonucleic acid (DNA) that alters expression of protooncogenes and tumor suppressor genes, as well as indirect mechanisms arising from cycles of cell turnover and regeneration in an inflamed tissue microenvironment.[42] This animal model has primarily been used to study the prevention and treatment of human HBV-induced HCC and to image

hepatic neoplasms, including PET.[41,43,44] A previous study of four animals identified PSMA expression in tumor-associated neovasculature in WHV-induced woodchuck HCC and demonstrated [^{68}Ga]Ga-PSMA-11 uptake on PET, suggesting additional utility of this model for evaluating PSMA-targeted theranostics.[43] We further characterized PSMA-targeted imaging and normal-tissue PSMA expression, including the salivary glands, in woodchucks with WHV-induced HCC. We also evaluated SSTR2/5 expression and [^{68}Ga]Ga-DOTATOC uptake and explored the feasibility and short-term tolerability of a single [^{177}Lu]Lu-PSMA-617 administration.

Results

Animals

Twelve animals (seven females and five males) with a median weight of 3.6 kg (range, 2.8 to 5.3 kg) were included in the study. The number of liver tumors >2 cm³ on CT at the time of PET imaging was one (n = 8), two (n = 3), or three (n = 1). One animal was enrolled before reaching the GGT threshold because ultrasound findings were highly suggestive of HCC.

The median volume of the largest CT-defined tumor was 32.9 cm³ (range, 5.0 to 126.4 cm³). Histopathology confirmed HCC in all animals (n = 6) that underwent needle biopsy.

RT-qPCR

RT-qPCR confirmed detectable PSMA transcripts in woodchuck HCC (n = 8 tumors) and SSTR2/5 transcripts (n = 7 tumors), with amplification also observed in liver (PSMA, SSTR2/5) and salivary gland tissue (PSMA) (Figure 1). In animals with matched liver and tumor samples, tumor PSMA expression was higher than liver in all tumor samples from two animals, whereas in

a third animal one tumor showed higher and one showed lower PSMA expression than matched liver. The highest tumor expression of SSTR2 and SSTR5 was observed in the animal with the highest [^{68}Ga]Ga-DOTATOC PET uptake.

[^{68}Ga]Ga-PSMA-11 PET Imaging

Regions of high and low [^{68}Ga]Ga-PSMA-11 uptake were observed within individual tumors relative to liver (Figure 2); uptake varied between animals. Tumor SUV_{max} ranged from 2.4 to 4.7 (median 3.3), and liver SUV_{mean} ranged from 1.4 to 2.6 (median 1.7), corresponding to a median tumor-to-liver ratio of 1.9. Uptake was observed in the spleen (Figure 2), as well as in the mandibular, temporal, and parotid salivary glands and testicles (Figure 3). Mandibular salivary gland SUV_{max} ranged from 2.3 to 3.3 (median 2.6) and testicular SUV_{max} ranged from 12.2 to 14.3 (median 12.2; n = 3 testicles).

[^{68}Ga]Ga-DOTATOC PET Imaging

Of six woodchucks, only one showed strong tumor uptake relative to liver on [^{68}Ga]Ga-DOTATOC PET imaging, with high peripheral and minimal central tumor uptake (Figure 2). Tumor SUV_{max} ranged from 3.0 to 14.2 (median 4.8), and liver SUV_{mean} ranged from 2.0 to 5.6 (median 4.2), corresponding to a median tumor-to-liver ratio of 1.2 (2.6 in the animal with strong tumor uptake). Uptake was present in the pancreas in all animals; the pancreas SUV_{max} ranged from 4.4 to 18.4 (median 8.6).

[^{64}Cu]Cu-PSMA-617 PET/CT Imaging and Exploratory [^{177}Lu]Lu-PSMA-617 Administration

Tumor SUV_{max} was higher at 24 hours post-injection of [^{64}Cu]Cu-PSMA-617 than at 4 hours post-injection in all animals. On gamma camera images acquired after injection of [^{177}Lu]Lu-PSMA-617, the radiotracer demonstrated initial uptake in the liver and heart, followed by accumulation in the kidney and bladder, consistent with systemic circulation and renal clearance (Figure 4). Uptake was observed in the mandibular salivary glands. Uptake in tumors was difficult to follow over time due to tumor superimposition on the liver and the motion of the tumor relative to the liver.

Platelet count and hemoglobin remained within reference intervals, and white blood cell count was within the reference interval except in one animal with elevated white blood cell count ($> 13.7 \times 10^9$/L) pre- and post-therapy. Creatinine and phosphorus remained within reference intervals except in one animal with elevated values before treatment; these values returned to within reference intervals at the 14-day follow-up. Total bilirubin and alanine transaminase remained within reference intervals in all animals. GGT (a known sensitive plasma biomarker of woodchuck HCC) increased from baseline at weeks 2 and 6 in all three animals. Alkaline phosphatase was within the reference range in all animals before treatment but was elevated in one animal at week 2 and two animals at week 6. Activity, appetite and body weight were monitored; no changes in appetite or activity were observed. Body weight was 2.9–19.9% below baseline at six weeks. The contribution of treatment to weight loss could not be distinguished from seasonal variation or tumor progression. Tumor volumes at baseline and 41–42 days were 13.6 and 27.8, 21.1 and 20.0, and 3.0 and 9.6 cm³ in the three animals, respectively.

Histology and IHC

The median survival time from diagnosis of HCC (GGT ≥ 50 U/L and a liver mass on ultrasound ≥ 2 cm in diameter) was 28.6 weeks (range, 4.1 to 37.4 weeks). HCC was confirmed in all animals by histopathological examination of tumor samples collected at necropsy (Figure 5). The number of liver tumors at the time of euthanasia was one (n = 3), two (n = 2), three (n = 4), and four, five and seven tumors in one animal each. Tumors frequently contained multinucleated cytomegalic cells**.** Metastatic spread to hepatic lymph nodes was diagnosed in 6 of 10 animals (lymph nodes were not sampled in two animals) and was confirmed by the presence of cytomegalic cells within the lymph node parenchyma (Figure 5). Biliary carcinoma was present within HCC in three animals.

The distribution of staining intensity across tissues for all antibodies is provided in Additional File 1. Cytoplasmic and membranous PSMA staining was present in salivary gland epithelial cells and testicles (Figure 6)**.** Positive staining was also observed in liver, spleen, kidney and prostate (Figure 7). IHC demonstrated cytoplasmic expression of both SSTR2 and SSTR5 across tumors. Strong SSTR2 and/or SSTR5 staining was observed in at least one tumor from five of six animals. In the remaining animal, tumor staining was weak for SSTR2 and moderate for SSTR5. Inter-tumoral heterogeneity was observed, with some lesions showing weak or absent expression. Positive staining was also observed for both SSTR2 and SSTR5 in liver and kidney.

Discussion

In this study, [^{68}Ga]Ga-PSMA-11 PET imaging in woodchuck HCC demonstrated heterogeneous intra- and intertumoral uptake, with a median tumor SUV_{max} of 3.3 and tumor-to-liver ratio of 1.9, with corresponding intratumoral variability in histopathology and PSMA

expression. Previous work demonstrated PSMA expression in tumor-associated neovasculature and [^{68}Ga]Ga-PSMA-11 uptake in woodchuck HCC.[43] The present study provides further characterization of PSMA-targeted imaging and normal-tissue expression, including the salivary glands, and adds evaluation of SSTR-targeted imaging and tissue expression, together with an exploratory assessment of [^{177}Lu]Lu-PSMA-617 administration. In human patients, heterogeneous uptake of ^{68}Ga-labelled PSMA ligands has been described in HCC tumors, with increased PET avidity in regions that showed contrast enhancement on arterial-phase CT imaging.[8,17,45] This uptake pattern may reflect intratumoral variability in perfusion, interstitial pressure, necrosis, fibrosis, and target expression.[36,37] Nonuniform radiopharmaceutical uptake may compromise targeted radiotherapy by causing variation in absorbed dose and potentially sparing cancer cells, reducing treatment effectiveness.[36]

Murine models using subcutaneous and orthotopic HCC xenografts show positive staining of tumor endothelium with PSMA-directed antibodies, and consistent, uniform tumor uptake on PET imaging after [^{68}Ga]Ga-PSMA-617.[46] High SPECT uptake and significant tumor growth suppression after [^{177}Lu]Lu-PSMA-617 have been reported in the subcutaneous xenograft model.[47] While useful in preclinical investigations of targeted radiotherapy for HCC, murine xenograft models do not replicate the barriers to effective therapy associated with large, heterogeneous, spontaneous tumors. Low to absent tumor uptake of [^{177}Lu]Lu-PSMA-617 on SPECT has been reported in human HCC patients despite high uptake of [^{68}Ga]Ga-PSMA-11 on PET, with progression of disease after therapy.[14,48] A recent dosimetry study of five patients with non-prostate cancers, including one patient with HCC, found rapid tumor clearance and low absorbed doses of [^{177}Lu]Lu-PSMA-617 despite high uptake on screening [^{68}Ga]Ga-PSMA-11 PET/CT.[49] The contrast between human and murine HCC uptake of the therapeutic radionuclide

and response to treatment highlights the need for models that better reproduce spontaneous tumor barriers to effective radiopharmaceutical targeting. Woodchuck tumors and associated neovasculature develop spontaneously following viral infection, and regions of necrosis, fibrosis and hemorrhage were identified in the woodchuck tumors in this study, similar to the heterogeneous histological features reported in human HBV-induced HCC.[50] PSMA staining varied intratumorally in the woodchuck tumors, as reported in human HCC.[9] Overall, the woodchuck tumors showed heterogeneous histopathology, target staining, and radiopharmaceutical uptake. These observations support the translational relevance of the woodchuck model for further studies of radiopharmaceutical delivery.

Physiologic uptake of PSMA-targeted radiopharmaceuticals was observed in woodchuck salivary glands on both [^{68}Ga]Ga-PSMA-11 PET (median SUV_{max} 2.6) and [^{177}Lu]Lu-PSMA-617 gamma camera imaging, with corresponding PSMA mRNA and protein expression confirmed by RT–qPCR and IHC. High PSMA-targeted radiopharmaceutical uptake in human salivary glands is well described[51,52], and 61% of human patients receiving [^{177}Lu]Lu-PSMA-617 in a phase 3 trial experienced xerostomia.[53] Unlike external beam radiation therapy, in which normal organ irradiation can be minimized, it is difficult to avoid irradiation of normal organs with high radiopharmaceutical uptake when targeted radiotherapy is used, as treatment is administered systemically. Most patients experience mild to moderate (grade 1 or 2), temporary symptoms; however, severe xerostomia may lead to dose reduction or permanent discontinuation of therapy.[53] The rate of treatment-related xerostomia may be even higher with alpha particle emitters[54], with up to one-quarter of patients requesting discontinuation of therapy due to this adverse effect.[55] Xerostomia is associated with an increased risk of dental caries and oral infection, oral discomfort, suboptimal nutrition and decreased quality of life.[56] Given the impact

on patients, strategies to mitigate xerostomia in human patients undergoing targeted radiotherapy are under investigation, with interventions mainly focused on reduction of radiopharmaceutical delivery to the salivary glands.[57] The exact mechanism of uptake of PSMA-targeting radiopharmaceuticals in the salivary glands is not clear, with some suggestion that a different protein, closely related to PSMA, may be responsible for the accumulation.[58] Some xerostomia prevention strategies have shown promise, but additional research is needed to address this common and impactful adverse effect of PSMA-targeted radiotherapy.

Murine models do not fulfill this need; PSMA expression is low in the salivary glands of mice compared to humans, and even lower in rats.[39] In contrast, PSMA mRNA and protein were detected in all mandibular salivary gland samples in woodchucks in this study, and salivary glands exhibited [^{68}Ga]Ga-PSMA-11 uptake on PET and [^{177}Lu]Lu-PSMA-617 uptake on gamma camera imaging, supporting use of this animal model for investigating mechanisms of salivary gland uptake and strategies to spare salivary glands in patients treated with PSMA-targeted radiotherapy.

PSMA expression in woodchuck normal tissues was confirmed by RT–qPCR and IHC, with corresponding physiologic uptake on [^{68}Ga]Ga-PSMA-11 PET, including the highest uptake in the testicles. PSMA expression was similar to that reported in humans, with PSMA mRNA expression in salivary gland and liver and protein expression in salivary gland, liver, kidney, prostate and testicles.[59,60] Stain was localized to similar cell types as reported for human tissues: salivary gland acinar and ductal epithelial cells[59,61], bile canaliculi of hepatocytes[9], proximal renal tubules[62,63], and prostate epithelial cells[64]. The cytoplasmic and membranous staining in the woodchuck testicle contrasts with the lack of staining reported in the human testicle in the Human Protein Atlas[65], although PSMA expression in human testicular seminiferous tubules has

been reported with IHC.[60] The pattern of uptake on [^{68}Ga]Ga-PSMA-11 PET reflected the PSMA expression on RT-qPCR and IHC. The testicles showed the highest PET uptake among all normal tissues quantified, in contrast to reports in human patients, where high uptake has been reported only with testicular infection and metastatic disease.[66,67]

SSTR2 and SSTR5 expression in normal woodchuck tissues was confirmed by RT–qPCR and IHC, with corresponding uptake on [^{68}Ga]Ga-DOTATOC PET demonstrating the highest physiologic uptake in the pancreas. Expression patterns across normal tissues were also similar to those in humans, with SSTR2 and SSTR5 mRNA expression in liver, and protein expression in liver, pancreas and kidney.[68] Cell types that stained were comparable to what is reported for human tissues: cytoplasmic staining of hepatocytes[69], the pancreatic islets[70], and the tubular epithelial cells.[71,72] Bile duct staining, which is reported in normal human liver, was not observed.[25] [^{68}Ga]Ga-DOTATOC PET showed uptake in these organs, with higher uptake in pancreas than liver; however, the high PET uptake in the spleen reported in humans after [^{68}Ga]Ga-DOTATOC administration was not observed in the woodchuck.[68,73]

Investigation into the feasibility of SSTR-targeted radionuclide therapy for human HCC is ongoing. Despite reports of radiolabeled somatostatin analogue uptake in patients with HCC[28-30], none of the 12 HCC participants in a completed [^{68}Ga]Ga-DOTATATE PET/MRI trial demonstrated somatostatin receptor positivity as defined by the study.[74] These findings suggest variability in SSTR-targeted tracer uptake among HCC tumors. In this animal cohort, strong [^{68}Ga]Ga-DOTATOC tumor uptake was seen in only one woodchuck, which also demonstrated the highest SSTR2 tumor mRNA expression and strong tumor staining intensity on SSTR2 IHC. This is consistent with variable SSTR2 expression reported in human HCC.[23,26,75] Although SSTR staining was present in most tumors, it was cytoplasmic and did not necessarily indicate

receptor expression at the cell surface. Tissue staining alone may therefore be insufficient to predict uptake of SSTR-targeted tracers.

Woodchuck HCCs were of clinically relevant size (median volume 32.9 cm^3) and demonstrated imaging characteristics consistent with human HCC on multiphasic CT. Tumor dimensions are comparable to those in humans, and serial monitoring allows selection of specific size ranges for study. The larger animal size permits use of clinical imaging modalities and equipment. Tumor features on arterial and delayed phase CT imaging are similar to human HCC, and human Liver Imaging Reporting and Data System criteria have been reported to have high sensitivity and specificity for detecting malignant tumors in the woodchuck liver.[76] The findings of this study suggest that pathological confirmation of woodchuck HCC before study inclusion may not be necessary in WHV-positive animals meeting imaging criteria; in this study, all liver masses ≥ 2 cm on ultrasound with CT features characteristic of HCC (arterial phase enhancement, venous phase washout, heterogeneous contrast uptake) were confirmed to be HCC on histopathology.

The larger animal size allows serial venipuncture for hematologic and organ toxicity assessment, and peripheral IV catheter placement for radiopharmaceutical or contrast administration. Samples can be reliably collected by venipuncture. All scheduled blood sampling and IV drug administration were successfully performed by a veterinarian using peripheral venous access without vascular access ports. The longer survival of tumor-bearing woodchucks compared to other laboratory animals allows assessment of response to therapy and delayed toxicity from radiation therapy. In three animals, a single [^{177}Lu]Lu-PSMA-617 administration and serial follow-up were feasible.

Limitations of the woodchuck model include the cost of animals and housing and the need for longitudinal monitoring of virus-positive animals because tumor development is not temporally synchronized across animals. In addition, woodchucks infected with woodchuck hepatitis virus develop chronic hepatitis and mild fibrosis, but do not progress to cirrhosis, and therefore do not model the possible changes in expression of PSMA and SSTR2 in cirrhosis.[25,41,77]

There were several limitations to this study, including the small sample size, which reduced our ability to capture inter-animal (including sex) variability. Antigen-specific binding as the mechanism of tumor radiopharmaceutical uptake could not be confirmed. Vascular PSMA localization was based on morphology without an endothelial marker, and associations between tissue features and tracer uptake were not assessed quantitatively. Prior [^{177}Lu]Lu-PSMA-617 administration in three animals may have affected subsequent [^{68}Ga]Ga-PSMA-11 uptake. A single administration of [^{177}Lu]Lu-PSMA-617 allowed an exploratory assessment of feasibility and short-term tolerability but was not designed to evaluate tumor response to therapy or cumulative organ toxicity. Lastly, SPECT-CT was not available for imaging the woodchucks after [^{177}Lu]Lu-PSMA-617 administration, and the uniformity of tumor uptake could not be accurately assessed with planar gamma camera imaging.

Conclusions

These findings support the WHV-induced HCC model for further studies of molecular imaging and target expression in spontaneous HCC. Antibodies developed against human PSMA and SSTR2/5 showed immunoreactivity in woodchuck tissues, and targeted radiotracers showed variable uptake in tumors and normal organs. Tumor biological behaviour resembled several

clinically relevant features of human HCC: multiple intrahepatic tumors were present in most animals at euthanasia, and metastatic spread to hepatic lymph nodes occurred in 6 of 10 animals in which lymph nodes were sampled.[78,79] Tumors showed intra- and intertumoral heterogeneity in contrast enhancement, fibrosis, and necrosis, all of which influence radiopharmaceutical uptake. These features may make the woodchuck-HCC model useful for investigating barriers to radiopharmaceutical delivery and developing strategies to improve tumor penetration and intratumoral distribution. Given the model's immune competence and spontaneous development of tumors *in situ*, it may also be valuable for studies of immunotherapy and interventions targeting the tumor microenvironment.

Materials and Methods

Animals

Twelve WHV-positive adult woodchucks (7 females, 5 males; exact ages unavailable) were accrued from the Western College of Veterinary Medicine colony. Animals were long-term residents of the institutional colony and were already acclimated to the housing environment before study procedures. Woodchucks were housed individually under a 12-hour light/dark cycle, with wood shavings and straw bedding, hiding shelters, and environmental enrichment including wood chews. Water was available ad libitum, and animals were provided a standard rabbit ration supplemented with fresh fruits and vegetables. Animals were visually assessed daily and underwent routine health monitoring by animal care staff and the facility veterinarian.

Colony animals were monitored with monthly serum biochemistry. Abdominal ultrasound was performed by a board-certified veterinary radiologist when gamma-glutamyl

transferase (GGT) reached ≥ 50 U/L or earlier if HCC was suspected. For six animals (4 females, 2 males) used for PSMA-targeted imaging, an ultrasound-guided needle biopsy of liver masses ≥ 2 cm in diameter was performed to confirm HCC. For six animals (3 females, 3 males) used for SSTR-targeted imaging, a presumptive diagnosis of HCC was made based on GGT ≥ 50 U/L and a liver mass ≥ 2 cm in diameter.80 The interval to euthanasia was calculated from the date on which both the GGT and ultrasound criteria were met. Animals with a hepatic mass suspicious for HCC present at the time each imaging study was conducted were included based on availability from the colony. Animals were not randomized to PSMA- or SSTR-targeted imaging. No additional exclusion criteria were applied, and no animals were excluded after enrolment.

As this was an exploratory study, a formal sample size calculation was not performed. Sample size was selected to allow assessment of inter-animal variability while minimizing animal use and was based on the number of eligible tumor-bearing woodchucks available from the institutional colony. The individual animal was the experimental unit. No separate control group was included because this was an exploratory study comparing imaging and tissue findings in animals with spontaneous WHV-induced HCC. All planned measurements were included in the analysis, except for one animal with repeat [^{64}Cu]Cu-PSMA-617 imaging, for which the second 4- and 24-hour measurements were used. Sample sizes varied where tissues or measurements were not obtained.

Pain control for needle biopsy was achieved with infiltration of the biopsy site with bupivacaine (0.3 mL; 5 mg/mL; SteriMax) and subcutaneous injection of meloxicam (0.2 mL/kg; Metacam 5 mg/mL, Boehringer Ingelheim Animal Health Canada, Burlington, ON, Canada). Isoflurane anesthesia was used for all procedures.

Quantitative Reverse Transcription Polymerase Chain Reaction (RT-qPCR)

Ribonucleic acid (RNA) was extracted from formalin-fixed, paraffin-embedded tissue specimens: tumor (n = 8 samples from 4 animals), liver (n = 5 samples from 5 animals), and mandibular salivary gland (n = 5 samples from 5 animals) for PSMA; tumor (n = 7 samples from 6 animals) and liver (n = 6 samples from 5 animals) for SSTR2; and tumor (n = 7 samples from 6 animals) and liver (n = 7 samples from 6 animals) for SSTR5, using a PureLink formalin-fixed, paraffin-embedded RNA Isolation Kit (Cat. No. K156002; ThermoFisher Scientific, Toronto, ON, Canada) according to the manufacturer's instructions. Total RNA (0.1 µg for each reaction) was used to generate complementary DNA with the Maxima First Strand complementary DNA Synthesis Kit for RT-qPCR (Cat. No. K1671; ThermoFisher Scientific, Toronto, ON, Canada). Primers for RT-qPCR were designed using the Custom TaqMan Gene Expression Assays VIC/FAM (Cat. No. 4448508, 4331348; ThermoFisher Scientific, Toronto, ON, Canada) based on Marmota monax messenger RNA (mRNA) sequences for an endogenous control gene glyceraldehyde-3-phosphate dehydrogenase (Gene ID 124078951; Comparative Toxicogenomic Database), PSMA (hypothetical predicted protein sequence KAF7476917.1, GenBank), SSTR2 (Gene ID 124105964; Comparative Toxicogenomics Database), and SSTR5 (Gene ID 124078406; Comparative Toxicogenomics Database). RT-qPCR was performed on a CFX96 Touch Real-Time PCR Detection System (Bio-Rad, Mississauga, ON, Canada) and the TaqMan Gene Expression Master Mix (Cat. No. 4370048; ThermoFisher Scientific, Toronto, ON, Canada). Expression data were obtained for each gene from each sample as a threshold cycle

(Ct). ΔCt was calculated as the Ct of the gene of interest (PSMA, SSTR2 or SSTR5) minus the Ct of the endogenous control gene.

Radiopharmaceuticals

[^{68}Ga]Ga-PSMA-11 was synthesized with an automated AllinOne radiochemistry module (Trasis, Ans, Belgium) using reagents, peptides, and cassettes provided by the vendor. ^{68}Ga was eluted from an IGG100 generator (Eckert & Ziegler Radiopharma GmbH, Berlin, Germany). The radiochemical purity of the final product was ≥ 97% as analyzed by reversed-phase high performance liquid chromatography and instant thin layer chromatography.

[^{64}Cu]Cu-PSMA-617 and [^{177}Lu]Lu-PSMA-617 were synthesized via established methods.81,82 [^{64}Cu]CuCl2 was purchased from the University of Alberta (Edmonton, AB, Canada), [^{177}Lu]LuCl3 was purchased from McMaster University (Hamilton, ON, Canada), and PSMA-617 was purchased from Selleckchem (Houston, TX, USA). Labeling was confirmed via instant thin-layer chromatography and radio high-performance liquid chromatography (Agilent, Santa Clara, CA, USA) using an Agilent Poroshell 120 EC-C18 2.7 μm 4.6 x 100 mm column. A gradient method starting at 90% H2O (with 0.1% trifluoroacetic acid) and 10% acetonitrile (with 0.1% trifluoroacetic acid) was utilized. Radiochemical purity was > 95%. [^{68}Ga]Ga-DOTATOC (DOTA-D-Phel-Tyr3-Octreotide) was synthesized with an automated AllinOne radiochemistry module (Trasis, Ans, Belgium) using reagents, peptides, and cassettes provided by the vendor. ^{68}Ga was eluted from an IGG100 generator (Eckert & Ziegler Radiopharma GmbH, Berlin, Germany). The

radiochemical purity of the final product was ≥ 97% as analyzed by reversed-phase high-performance liquid chromatography and instant thin-layer chromatography.

[^{68}Ga]Ga-PSMA-11 and [^{68}Ga]Ga-DOTATOC PET/CT Imaging

[^{68}Ga]Ga-PSMA-11 (n = 6) and [^{68}Ga]Ga-DOTATOC (n = 6) PET/CT scans were acquired with a 64-slice PET/CT scanner (Discovery MI Digital Ready, GE Medical Systems). Multiphasic CT scans were acquired before and 15-20, 30, 60, and 120 seconds after injection of 2 mL/kg iodine contrast (Omnipaque 350 mg/ml, GE Healthcare Canada) through a 24-gauge intravenous catheter placed in the cephalic or medial saphenous vein; arterial phase timing varied with injection duration. 5 mL/kg/hr of 0.9% NaCl was administered intravenously while under anesthesia for PET/CT imaging. PET scans were acquired 60 minutes after IV injection of [^{68}Ga]Ga-PSMA-11 (35.8, 37.8, 40, 40.5, 42, 44 MBq), and 60 minutes after IV injection of 4.2 MBq/kg [^{68}Ga]Ga-DOTATOC. Tumor volume was determined from the CT images; in animals with more than one tumor, the volume of the largest CT-defined tumor was used. Maximum and mean standardized uptake value (SUV) were calculated for tumor and liver (all animals), mandibular salivary gland and testicle ([^{68}Ga]Ga-PSMA-11 animals), and pancreas ([^{68}Ga]Ga-DOTATOC animals) from contours of the entire structure of interest on registered PET/CT scans (Eclipse version 13.6, Varian Medical Systems). In animals with more than one tumor, the SUV measurements were made on the tumor with the highest volume. Tumor-to-liver ratios were calculated as tumor SUV_{max} divided by liver SUV_{mean}. Three animals that had undergone [^{64}Cu]Cu-PSMA-617 PET/CT and a single [^{177}Lu]Lu-PSMA-617 administration were subsequently included in the [^{68}Ga]Ga-PSMA-11 imaging group because tumor uptake on

copper imaging was lower than expected. Gallium imaging was performed 70, 71, and 95 days after lutetium administration, with no intervening treatment.

[^{64}Cu]Cu-PSMA-617 PET/CT Imaging and Exploratory [^{177}Lu]Lu-PSMA-617 Administration

PET/CT scans were acquired for three animals (one female and two males), 4 and 24 hours after IV injection of [^{64}Cu]Cu-PSMA-617 (18.4, 19.3 and 29.2 MBq). One animal underwent an additional [^{64}Cu]Cu-PSMA-617 administration because little uptake was observed after the first imaging; for this animal, the 4- and 24-hour measurements from the second administration were used in the reported analysis. Tumor SUVmax was determined from registered PET/CT images using the same contouring approach described above. PET/CT scans were followed 5-7 days later by a single administration of [^{177}Lu]Lu-PSMA-617. [^{177}Lu]Lu-PSMA-617 (710, 718, and 729 MBq) was injected via a 24-gauge intravenous catheter over 60 minutes. Gamma camera images were acquired every 20 minutes for 120 minutes after injection. 100 mL of 0.9% NaCl was administered subcutaneously 4 hours before [^{177}Lu]Lu-PSMA-617 therapy, and 5 mL/kg/h of 0.9% NaCl was administered while under anesthesia. To monitor for hematopoietic and renal adverse effects, complete blood cell counts were collected before and 2 weeks after [^{177}Lu]Lu-PSMA-617, and serum biochemistries were collected before, and 2 and 6 weeks after treatment. Hematology and serum chemistry results were interpreted using available laboratory reference intervals for Marmota monax provided by the Calgary Zoo, Garden & Prehistoric Park (January 2022 version). Multiphasic CT scans were acquired 2 and 6 weeks after [^{177}Lu]Lu-PSMA-617.

Histology and IHC

Animals were monitored using a predefined humane intervention point checklist based on activity and responsiveness, feed and water intake, body weight, and physical appearance. Animals were euthanized if they developed a severe abnormality in any individual category, including severe depression or immobility, anorexia for 72 hours, >20% body weight loss, or a pre-moribund or moribund condition. A cumulative score >2 prompted review by the principal investigator. For euthanasia, general anesthesia was induced with mask-delivered isoflurane, followed by intravenous (IV) administration of T-61 euthanasia solution according to the manufacturer's instructions. A full necropsy examination was performed on all animals (n = 12), and the following tissue samples were collected into formalin: tumor(s), liver, hepatic lymph nodes, kidneys, small intestine, spleen, salivary glands, prostate, and testicles. Additional grossly abnormal tissues were also collected. Formalin-fixed tissue samples were embedded in paraffin blocks. Contiguous sections were cut and deparaffinized for hematoxylin and eosin (H&E) and IHC staining.

For animals that underwent PSMA-targeted imaging, IHC was performed using two mouse monoclonal antibodies against PSMA (antibody 1: 1:25 dilution, Cat. No. PSMA-L, clone 1D6; Leica Biosystems, Concord, ON, Canada, antibody 2: 1:100 dilution, Cat. No. MABN2300, clone 3F11; MilliporeSigma Canada, Oakville, ON, Canada). Commercial human PSMA-positive tissues (Cat. No. BSB-9358-CS; BioSB, Santa Barbara, CA, USA), canine prostate, and Marmota monax testicle tissues were used for positive controls in protocol development. The primary antibodies were detected using an anti-mouse EnVision+ System Horseradish peroxidase (HRP) Labeled Polymer and Liquid 3,3′-

Diaminobenzidine (DAB)+ Substrate Chromogen System (Cat. Nos. K4000 and K3468, Agilent Technologies Canada, Mississauga, ON, Canada) and Mouse and Rabbit Specific HRP/DAB IHC Detection Kit (Cat. No. ab236466; Abcam, Waltham, MA, USA). Negative controls were processed identically except that the primary antibody was omitted and sections were incubated with diluent buffer alone.

For animals that underwent DOTATOC-targeted imaging, IHC was performed using a rabbit monoclonal antibody against Somatostatin Receptor 2 (1:200 dilution, Cat. No. ab134152, clone UMB1; Abcam, Waltham, MA, USA) and a rabbit polyclonal antibody against Somatostatin Receptor 5 (1:1500 dilution, Cat. No. PA3-209; ThermoFisher Scientific, Toronto, ON, Canada). Marmota monax pancreas tissue was used as a positive control in protocol development. The primary antibodies were detected using a mouse and rabbit-specific HRP/DAB IHC Detection Kit (Cat. No. ab236466; Abcam, Waltham, MA, USA). Negative controls were processed identically as above.

Staining intensity was evaluated via light microscopy and scored semi-quantitatively as absent, weak, moderate, or strong by a veterinary graduate student under the supervision of an American College of Veterinary Pathology Diplomate. Histology was interpreted by the same pathologist.

Statistical Analysis

No statistical comparisons were performed because of the exploratory nature of the study and limited sample size; data are presented descriptively as median and range. Investigators were not blinded to imaging groups during allocation, experimental procedures, data analysis, or outcome assessment.

List of abbreviations

CT: Computed tomography

Ct: Threshold cycle

DAB: 3,3′-Diaminobenzidine

DNA: Deoxyribonucleic acid

GGT: Gamma-glutamyl transferase

H&E: Hematoxylin and eosin

HBV: Hepatitis B virus

HCC: Hepatocellular carcinoma

HRP: Horseradish peroxidase

IHC: Immunohistochemistry

IV: Intravenous

mRNA: Messenger RNA

PET: Positron emission tomography

PSMA: Prostate-specific membrane antigen

RNA: Ribonucleic acid

RT-qPCR: Quantitative reverse transcription polymerase chain reaction

SPECT: Single-photon emission computed tomography

SSTR: Somatostatin receptor

SSTR2: Somatostatin receptor subtype 2

SSTR5: Somatostatin receptor subtype 5

SUV: Standardized uptake value

SUV_{max}: Maximum standardized uptake value

SUV_{mean}: Mean standardized uptake value

WHV: Woodchuck hepatitis virus

ΔCt: Difference between target-gene and endogenous-control threshold cycles

Declarations

Ethics approval and consent to participate

Animal use was under an approved protocol and standard operating procedures established by the University of Saskatchewan Animal Research Ethics Board (AUP-20220105).

Consent for publication

Not applicable.

Availability of data and material

The numerical data underlying the analyses and figures in this study are provided in Additional File 1. The imaging datasets used and/or analysed during the current study are available from the corresponding author on reasonable request.

Competing interests

The authors declare that they have no competing interests.

Funding

593 This work was supported by a College of Medicine Research Award (CoMRAD), University of
594 Saskatchewan, and a Research Grant from the Canadian Association of Medical Radiation
595 Technologists (CAMRT). The University of Saskatchewan woodchuck colony included animals
596 supported through a Canadian Institutes of Health Research grant awarded to C.S.C. (Funding
597 Reference Number 180234). [^{68}Ga]Ga-PSMA-11 and [^{68}Ga]Ga-DOTATOC were provided in
598 kind by the laboratory of H.F. The funding organizations had no role in study design, data
599 collection, analysis, interpretation, or preparation of the manuscript.
600

601 Authors' contributions

602 H.P. contributed to study design, investigation, data curation and analysis, IHC scoring, and
603 preparation of the original manuscript draft. M.N.M. conceived and designed the study,
604 contributed to funding acquisition and ethics approval, investigation, data curation and analysis,
605 supervised the graduate student, and substantially revised the manuscript. S.L.S. performed
606 ultrasound imaging, ultrasound-guided biopsy and imaging interpretation. E.D. contributed to
607 study conceptualization, supervised radiochemistry for [^{64}Cu]Cu-PSMA-617 and [^{177}Lu]Lu-
608 PSMA-617, and served on the graduate student advisory committee. H.F. contributed to study
609 conceptualization, supervised radiochemistry for [^{68}Ga]Ga-PSMA-11 and [^{68}Ga]Ga-DOTATOC,
610 and provided these radiopharmaceuticals for the study. S.W. contributed to study
611 conceptualization, acquired funding for the initial PSMA studies, contributed to imaging
612 analysis, and served on the graduate student advisory committee. B.K.W. performed
613 histopathologic and IHC interpretation, supervised IHC scoring, and served on the graduate
614 student advisory committee. M.H. acquired funding for the DOTATOC studies, administered
615 radiopharmaceuticals, acquired PET imaging, and advised on SUV measurements. V.K.

contributed to data interpretation. A.D. performed the production, dispensing and quality control of [^{68}Ga]Ga-PSMA-11 and [^{68}Ga]Ga-DOTATOC in the Fonge laboratory. K.J.H.A. designed and performed the radiochemical labeling process for [^{64}Cu]Cu-PSMA-617 and [^{177}Lu]Lu-PSMA-617 in the Dadachova laboratory. C.S.C. contributed to study conceptualization, provided woodchucks, and served on the graduate student advisory committee. All authors contributed to study design and data interpretation, and reviewed and approved the final manuscript.

Acknowledgements

The authors thank LaRhonda Bren for performing the RT–qPCR assays, supporting RT–qPCR methodology and reviewing the relevant Methods section, and Karen Davis, RT(T), BSc(T), CMD, for performing image contouring and contributing expertise in image transfer between software platforms.

Additional file 1. Supplementary study data

Format: .xlsx

Description: Individual animal information, imaging measurements, necropsy findings, immunohistochemistry scores, RT-qPCR values, blood test results and reference intervals, and longitudinal tumor volumes and body weights.

References

1. Sung H, Ferlay J, Siegel RL, Laversanne M, Soerjomataram I, Jemal A, et al. Global cancer statistics 2020: GLOBOCAN estimates of incidence and mortality worldwide for 36 cancers in 185 countries. CA Cancer J Clin. 2021;71:209–249.
2. Petrick JL, Florio AA, Znaor A, Ruggieri D, Laversanne M, Alvarez CS, et al. International trends in hepatocellular carcinoma incidence, 1978–2012. Int J Cancer. 2020;147:317–330.
3. Sukowati CH, El-Khobar KE, Ie SI, Anfuso B, Muljono DH, Tiribelli C. Significance of hepatitis virus infection in the oncogenic initiation of hepatocellular carcinoma. World J Gastroenterol. 2016;22:1497–1512.
4. Jemal A, Ward EM, Johnson CJ, Cronin KA, Ma J, Ryerson B, et al. Annual report to the nation on the status of cancer, 1975–2014, featuring survival. J Natl Cancer Inst. 2017;109:djx030.
5. Zhang S, Wang X, Gao X, Chen X, Li L, Li G, et al. Radiopharmaceuticals and their applications in medicine. Signal Transduct Target Ther. 2025;10:1.
6. Tran HH, Yamaguchi A, Manning HC. Radiotheranostic landscape: a review of clinical and preclinical development. Eur J Nucl Med Mol Imaging. 2025;52:2685–2709.
7. Jiao D, Li Y, Yang F, Han D, Wu J, Shi S, et al. Expression of prostate-specific membrane antigen in tumor-associated vasculature predicts poor prognosis in hepatocellular carcinoma. Clin Transl Gastroenterol. 2019;10:1–7.
8. Kesler M, Levine C, Hershkovitz D, Mishani E, Menachem Y, Lerman H, et al. ^{68}Ga-PSMA is a novel PET-CT tracer for imaging of hepatocellular carcinoma: a prospective pilot study. J Nucl Med. 2019;60:185–191.

9. Tolkach Y, Goltz D, Kremer A, Ahmadzadehfar H, Bergheim D, Essler M, et al. Prostate-specific membrane antigen expression in hepatocellular carcinoma: potential use for prognosis and diagnostic imaging. Oncotarget. 2019;10:4149–4160.
10. Kunikowska J, Cieślak B, Gierej B, Patkowski W, Kraj L, Kotulski M, et al. [^{68}Ga]Ga-prostate-specific membrane antigen PET/CT: a novel method for imaging patients with hepatocellular carcinoma. Eur J Nucl Med Mol Imaging. 2021;48:883–892.
11. Alipour R, Gupta S, Trethewey S. ^{68}Ga-PSMA uptake in combined hepatocellular cholangiocarcinoma with skeletal metastases. Clin Nucl Med. 2017;42:e452–e453.
12. Das J, Ray S, Tapadia R, Midha D, Mallick I. Prostate-specific membrane antigen-expressing hepatic lesion: metastatic or hepatocellular carcinoma. Indian J Nucl Med. 2020;35:58–60.
13. Erhamamci S, Aslan N. Primary hepatocellular carcinoma with intense ^{68}Ga-PSMA uptake but slight 18F-FDG uptake on PET/CT imaging. Clin Nucl Med. 2020;45:e176–e177.
14. Hirmas N, Leyh C, Sraieb M, Barbato F, Schaarschmidt BM, Umutlu L, et al. ^{68}Ga-PSMA-11 PET/CT improves tumor detection and impacts management in patients with hepatocellular carcinoma. J Nucl Med. 2021;62:1235–1241.
15. Kuyumcu S, Has-Simsek D, Iliaz R, Sanli Y, Buyukkaya F, Akyuz F, et al. Evidence of prostate-specific membrane antigen expression in hepatocellular carcinoma using ^{68}Ga-PSMA PET/CT. Clin Nucl Med. 2019;44:702–706.
16. Patel D, Loh H, Le K, Stevanovic A, Mansberg R. Incidental detection of hepatocellular carcinoma on ^{68}Ga-labeled prostate-specific membrane antigen PET/CT. Clin Nucl Med. 2017;42:881–884.
17. Perez PM, Flavell RR, Kelley RK, Umetsu S, Behr SC. Heterogeneous uptake of 18F-FDG and ^{68}Ga-PSMA-11 in hepatocellular carcinoma. Clin Nucl Med. 2019;44:e133–e135.

18. Taneja S, Taneja R, Kashyap V, Jha A, Jena A. ^{68}Ga-PSMA uptake in hepatocellular carcinoma. Clin Nucl Med. 2017;42:e69–e70.

19. Qin C, Song X, Sun S, Song Y, Ruan W, Gai Y, et al. [^{68}Ga]Ga-PSMA-617 PET/MRI for imaging patients suspected of hepatocellular carcinoma. Eur J Nucl Med Mol Imaging. 2025;52:1278–1290.

20. Mei X, Li Y, Xu S, Shang X, Cheng B, Niu X, et al. 18F-PSMA-1007 versus 18F-FDG PET/CT in the detection of hepatocellular carcinoma. Front Oncol. 2025;15:1711398.

21. Catalano OA, Bhan I, Asmundo L, Bradley WR, Fonderico M, Zhang ML, et al. Diagnostic performance of PSMA PET/MRI in characterizing LI-RADS 3 observations in patients with cirrhosis. J Nucl Med. 2026;67:521–527.

22. Pauwels E, Cleeren F, Bormans G, Deroose CM. Somatostatin receptor PET ligands—the next generation for clinical practice. Am J Nucl Med Mol Imaging. 2018;8:311–331.

23. Lequoy M, Desbois-Mouthon C, Wendum D, Gupta V, Blachon JL, Scatton O, et al. Somatostatin receptors in resected hepatocellular carcinoma: status and correlation with markers of poor prognosis. Histopathology. 2017;70:492–498.

24. Liu Y, Jiang L, Mu Y. Somatostatin receptor subtypes 2 and 5 are associated with better survival in operable hepatitis B-related hepatocellular carcinoma following octreotide long-acting release treatment. Oncol Lett. 2013;6:821–828.

25. Reynaert H, Rombouts K, Vandermonde A, Urbain D, Kumar U, Bioulac-Sage P, et al. Expression of somatostatin receptors in normal and cirrhotic human liver and in hepatocellular carcinoma. Gut. 2004;53:1180–1189.

26. Bläker M, Schmitz M, Gocht A, Burghardt S, Schulz M, Bröring DC, et al. Differential expression of somatostatin receptor subtypes in hepatocellular carcinomas. J Hepatol. 2004;41:112–118.
27. Verhoef C, van Dekken H, Hofland LJ, Zondervan PE, de Wilt JH, van Marion R, et al. Somatostatin receptor in human hepatocellular carcinomas: biological, patient and tumor characteristics. Dig Surg. 2008;25:21–26.
28. Tabacchi E, Campana D, Brighi N, Fanti S, Ambrosini V. ^{68}Ga-DOTANOC PET/CT detects multifocal hepatocellular carcinoma. Clin Nucl Med. 2019;44:238–239.
29. Ulaner GA, Bodei L. Hepatocellular carcinoma mimicking neuroendocrine tumor metastasis on ^{68}Ga-DOTATATE PET/CT. Clin Nucl Med. 2019;44:330–331.
30. Momeny M, AghaAmiri S, Hernandez Vargas S, Acidi B, Ghosh SC, Bateman TM, et al. SSTR2-targeted theranostics in hepatocellular carcinoma. Cancers (Basel). 2025;17:162.
31. Bokhout L, Campeiro JD, Dalm SU. Exploring the landscape of current in vitro and in vivo models and their relevance for targeted radionuclide theranostics. Eur J Nucl Med Mol Imaging. 2025;52:3291–3311.
32. Kleynhans J, Ebenhan T, Cleeren F, Sathekge MM. Can current preclinical strategies for radiopharmaceutical development meet the needs of targeted alpha therapy? Eur J Nucl Med Mol Imaging. 2024;51:1965–1980.
33. Landgraf M, McGovern JA, Friedl P, Hutmacher DW. Rational design of mouse models for cancer research. Trends Biotechnol. 2018;36:242–251.
34. Zhang W, Fan W, Rachagani S, Zhou Z, Lele SM, Batra SK, et al. Comparative study of subcutaneous and orthotopic mouse models of prostate cancer: vascular perfusion, vasculature density, hypoxic burden and BB2r-targeting efficacy. Sci Rep. 2019;9:11117.

35. van der Heide CD, Dalm SU. Radionuclide imaging and therapy directed towards the tumor microenvironment: a multi-cancer approach for personalized medicine. Eur J Nucl Med Mol Imaging. 2022;49:4616–4641.
36. Mellhammar E, Dahlbom M, Vilhelmsson-Timmermand O, Strand SE. Tumor control probability and small-scale Monte Carlo dosimetry: effects of heterogenous intratumoral activity distribution in radiopharmaceutical therapy. J Nucl Med. 2023;64:1632–1637.
37. Echavidre W, Fagret D, Faraggi M, Picco V, Montemagno C. Recent pre-clinical advancements in nuclear medicine: pioneering the path to a limitless future. Cancers (Basel). 2023;15:4839.
38. Huang X, Bennett M, Thorpe PE. Anti-tumor effects and lack of side effects in mice of an immunotoxin directed against human and mouse prostate-specific membrane antigen. Prostate. 2004;61:1–11.
39. Roy J, Warner BM, Basuli F, Zhang X, Wong K, Pranzatelli T, et al. Comparison of prostate-specific membrane antigen expression levels in human salivary glands to non-human primates and rodents. Cancer Biother Radiopharm. 2020;35:284–291.
40. Meyer C, Stuparu A, Lueckerath K, Calais J, Czernin J, Slavik R, et al. Tandem isotope therapy with 225Ac- and ^{177}Lu-PSMA-617 in a murine model of prostate cancer. J Nucl Med. 2023;64:1772–1778.
41. Tennant BC, Toshkov IA, Peek SF, Jacob JR, Menne S, Hornbuckle WE, et al. Hepatocellular carcinoma in the woodchuck model of hepatitis B virus infection. Gastroenterology. 2004;127:S283–S293.
42. Tennant BC, Gerin JL. The woodchuck model of hepatitis B virus infection. ILAR J. 2001;42:89–102.

751 43. Sergeeva O, Zhang Y, Julian W, Sasikumar A, Awadallah A, Kenyon J, et al. Imaging of
752 tumor-associated vascular prostate-specific membrane antigen in woodchuck model of
753 hepatocellular carcinoma. Gastro Hep Adv. 2022;1:631–639.
754 44. Cao W, Sergeeva O, Julian W, Kresak A, Lusinger D, Schneider J, et al. PET imaging of
755 hepatocellular carcinoma with [124I]IV-14. EJNMMI Res. 2025;15:35.
756 45. Muzaffar S, Ahmed N, Rahman U, Al Kandari F, Usmani S. ^{68}Ga-prostate-specific
757 membrane antigen uptake as a surrogate biomarker of neovascularity in hepatocellular
758 carcinoma. Indian J Nucl Med. 2021;36:90–91.
759 46. Lu Q, Long Y, Fan K, Shen Z, Gai Y, Liu Q, et al. PET imaging of hepatocellular carcinoma
760 by targeting tumor-associated endothelium using [^{68}Ga]Ga-PSMA-617. Eur J Nucl Med Mol
761 Imaging. 2022;49:4000–4013.
762 47. Lu Q, Long Y, Gai Y, Liu Q, Jiang D, Lan X. [^{177}Lu]Lu-PSMA-617 theranostic probe for
763 hepatocellular carcinoma imaging and therapy. Eur J Nucl Med Mol Imaging. 2023;50:2342–
764 2352.
765 48. Pretet V, Giraudet AL, Vergnaud L, Paquet E, Kryza D. Radionuclide therapy with ^{177}Lu-
766 PSMA in a patient with hepatocellular carcinoma. Clin Nucl Med. 2024;49:584–586.
767 49. Khreish F, Rosar F, Burgard C, Petto S, Maus S, Stemler T, et al. Dosimetric analysis reveals
768 rapid clearance and low absorbed dose of [^{177}Lu]Lu-PSMA-617 in non-prostate cancers with
769 high PSMA expression. EJNMMI Res. 2026;16:49.
770 50. Zheng W, Haw Y, Wang HL. Advances in hepatocellular carcinoma: molecular insights,
771 histologic subtypes, and differential diagnosis. Adv Anat Pathol. 2025;32:317–326.
772 51. Afshar-Oromieh A, Malcher A, Eder M, Eisenhut M, Linhart HG, Hadaschik BA, et al. PET
773 imaging with a [^{68}Ga]gallium-labelled PSMA ligand for the diagnosis of prostate cancer:

biodistribution in humans and first evaluation of tumour lesions. Eur J Nucl Med Mol Imaging. 2013;40:486–495.

52. Klein Nulent TJW, Valstar MH, de Keizer B, Willems SM, Smit LA, Al-Mamgani A, et al. Physiologic distribution of PSMA-ligand in salivary glands and seromucous glands of the head and neck on PET/CT. Oral Surg Oral Med Oral Pathol Oral Radiol. 2018;125:478–486.
53. Fizazi K, Chi KN, Shore ND, Herrmann K, de Bono JS, Castellano D, et al. Final overall survival and safety analyses of the phase III PSMAfore trial of [^{177}Lu]Lu-PSMA-617 versus change of androgen receptor pathway inhibitor in taxane-naive patients with metastatic castration-resistant prostate cancer. Ann Oncol. 2025;36:1319–1330.
54. Sathekge MM, Lawal IO, Bal C, Bruchertseifer F, Ballal S, Cardaci G, et al. Actinium-225-PSMA radioligand therapy of metastatic castration-resistant prostate cancer (WARMTH Act): a multicentre, retrospective study. Lancet Oncol. 2024;25:175–183.
55. Feuerecker B, Tauber R, Knorr K, Heck M, Beheshti A, Seidl C, et al. Activity and adverse events of actinium-225-PSMA-617 in advanced metastatic castration-resistant prostate cancer after failure of lutetium-177-PSMA. Eur Urol. 2021;79:343–350.
56. Jensen SB, Pedersen AM, Vissink A, Andersen E, Brown CG, Davies AN, et al. A systematic review of salivary gland hypofunction and xerostomia induced by cancer therapies: prevalence, severity and impact on quality of life. Support Care Cancer. 2010;18:1039–1060.
57. Muniz M, Loprinzi CL, Orme JJ, Koch RM, Mahmoud AM, Kase AM, et al. Salivary toxicity from PSMA-targeted radiopharmaceuticals: what we have learned and where we are going. Cancer Treat Rev. 2024;127:102748.

58. Rupp NJ, Umbricht CA, Pizzuto DA, Lenggenhager D, Töpfer A, Müller J, et al. First clinicopathologic evidence of a non-PSMA-related uptake mechanism for ^{68}Ga-PSMA-11 in salivary glands. J Nucl Med. 2019;60:1270–1276.
59. Nishida H, Kondo Y, Kusaba T, Kadowaki H, Daa T. Immunohistochemical reactivity of prostate-specific membrane antigen in salivary gland tumors. Head Neck Pathol. 2022;16:427–433.
60. Kinoshita Y, Kuratsukuri K, Landas S, Imaida K, Rovito PM Jr, Wang CY, et al. Expression of prostate-specific membrane antigen in normal and malignant human tissues. World J Surg. 2006;30:628–636.
61. Voter AF, Amindarolzarbi A, Shen CJ, Wang J, Kang H, Sharma R, et al. A pilot study of PSMA-targeted F-18-DCFPyL PET imaging of patients with adenoid cystic carcinoma. Sci Rep. 2025;15:17104.
62. Baccala A, Sercia L, Li J, Heston W, Zhou M. Expression of prostate-specific membrane antigen in tumor-associated neovasculature of renal neoplasms. Urology. 2007;70:385–390.
63. Al-Ahmadie HA, Olgac S, Gregor PD, Tickoo SK, Fine SW, Kondagunta GV, et al. Expression of prostate-specific membrane antigen in renal cortical tumors. Mod Pathol. 2008;21:727–732.
64. Silver DA, Pellicer I, Fair WR, Heston WD, Cordon-Cardo C. Prostate-specific membrane antigen expression in normal and malignant human tissues. Clin Cancer Res. 1997;3:81–85.
65. Uhlén M, Fagerberg L, Hallström BM, Lindskog C, Oksvold P, Mardinoglu A, et al. Tissue expression of FOLH1 – Testis. The Human Protein Atlas. https://v21.proteinatlas.org/ENSG00000086205-FOLH1/tissue/testis. Accessed 19 October 2026.

66. Calderon Tobar MN, Önner H. ^{68}Ga-PSMA uptake in the testis: two different patients with two different diagnosis. Clin Nucl Med. 2024;49:578–579.
67. de Oliveira Taveira M, Razmaria AA, Schoder H, Yeh R. Prostate cancer recurrence due to isolated testicular metastases detected by PSMA PET/CT. J Nucl Med. 2025;66:892–895.
68. Boy C, Heusner TA, Poeppel TD, Redmann-Bischofs A, Unger N, Jentzen W, et al. ^{68}Ga-DOTATOC PET/CT and somatostatin receptor (sst1–sst5) expression in normal human tissue: correlation of sst2 mRNA and SUVmax. Eur J Nucl Med Mol Imaging. 2011;38:1224–1236.
69. Uhlén M, Fagerberg L, Hallström BM, Lindskog C, Oksvold P, Mardinoglu A, et al. Tissue expression of SSTR2 – Liver. The Human Protein Atlas. https://www.proteinatlas.org/ENSG00000180616-SSTR2/tissue/liver#img. Accessed 19 October 2026.
70. Taniyama Y, Suzuki T, Mikami Y, Moriya T, Satomi S, Sasano H. Systemic distribution of somatostatin receptor subtypes in human: an immunohistochemical study. Endocr J. 2005;52:605–611.
71. Bhandari S, Watson N, Long E, Sharpe S, Zhong W, Xu SZ, et al. Expression of somatostatin and somatostatin receptor subtypes 1–5 in human normal and diseased kidney. J Histochem Cytochem. 2008;56:733–743.
72. Kulaksiz H, Eissele R, Rössler D, Schulz S, Höllt V, Cetin Y, et al. Identification of somatostatin receptor subtypes 1, 2A, 3, and 5 in neuroendocrine tumours with subtype specific antibodies. Gut. 2002;50:52–60.

73. Kulkarni HR, Prasad V, Kaemmerer D, Hommann M, Baum RP. High uptake of ^{68}Ga-DOTATOC in spleen as compared to splenosis: measurement by PET/CT. Recent Results Cancer Res. 2013;194:373–378.

74. ClinicalTrials.gov. [^{68}]Ga-DOTATATE PET/MRI in hepatocellular carcinoma (NCT03648073). https://clinicaltrials.gov/study/NCT03648073. Accessed 19 October 2026.

75. Kaemmerer D, Schindler R, Mußbach F, Dahmen U, Altendorf-Hofmann A, Dirsch O, et al. Somatostatin and CXCR4 chemokine receptor expression in hepatocellular and cholangiocellular carcinomas: tumor capillaries as promising targets. BMC Cancer. 2017;17:896.

76. Mauda-Havakuk M, Mikhail AS, Starost MF, Jones EC, Karim B, Kleiner DE, et al. Imaging, pathology, and immune correlates in the woodchuck hepatic tumor model. J Hepatocell Carcinoma. 2021;8:71–83.

77. Chen LX, Zou SJ, Li D, Zhou JY, Cheng ZT, Zhao J, et al. Prostate-specific membrane antigen expression in hepatocellular carcinoma, cholangiocarcinoma, and liver cirrhosis. World J Gastroenterol. 2020;26:7664–7678.

78. Feo F, Pascale RM. Multifocal hepatocellular carcinoma: intrahepatic metastasis or multicentric carcinogenesis? Ann Transl Med. 2015;3:4.

79. Amini N, Ejaz A, Spolverato G, Maithel SK, Kim Y, Pawlik TM. Management of lymph nodes during resection of hepatocellular carcinoma and intrahepatic cholangiocarcinoma: a systematic review. J Gastrointest Surg. 2014;18:2136–2148.

80. Jacob JR, Sterczer A, Toshkov IA, Yeager AE, Korba BE, Cote PJ, et al. Integration of woodchuck hepatitis and N-myc rearrangement determine size and histologic grade of hepatic tumors. Hepatology. 2004;39:1008–1016.

81. Cui C, Hanyu M, Hatori A, Zhang Y, Xie L, Ohya T, et al. Synthesis and evaluation of [^{64}Cu]PSMA-617 targeted for prostate-specific membrane antigen in prostate cancer. Am J Nucl Med Mol Imaging. 2017;7:40–52.

82. Kristiansson, A, Örbom, A, Ahlstedt, J, Karlsson, H, Zedan, W, Gram, M, et al. ^{177}Lu-PSMA-617 therapy in mice, with or without the antioxidant α1-microglobulin (A1M), including kidney damage assessment using 99mTc-MAG3 imaging. Biomolecules. 2021;11:263.

886 **Figure 1.** Detection of PSMA and SSTR2/5 transcripts in woodchuck tissues by RT-qPCR. RT-
887 qPCR analysis of (A) PSMA, (B) SSTR2, and (C) SSTR5 mRNA in formalin-fixed, paraffin-
888 embedded tissues from woodchucks with hepatocellular carcinoma. ΔCt values are normalized to
889 the endogenous control gene glyceraldehyde-3-phosphate dehydrogenase. Each point represents
890 an individual tissue sample; horizontal bars indicate group medians. The asterisk (*) in (B)
891 indicates the ΔCt value of the animal with the highest uptake of [^{68}Ga]Ga-DOTATOC on PET
892 imaging.
893
894 **Figure 2**. Whole-body PET/CT imaging of woodchucks with WHV-induced hepatocellular
895 carcinoma. Imaging was acquired 1h post [^{68}Ga]Ga-PSMA-11 (A-C) and [^{68}Ga]Ga-DOTATOC
896 (D-F). (A) Three-dimensional maximum intensity projection PET image demonstrating focal
897 tracer uptake within the hepatic tumor (white arrows) relative to surrounding liver (black
898 arrows). (B) Fused coronal PET and delayed phase (60 seconds) contrast-enhanced CT images
899 show higher [^{68}Ga]Ga-PSMA-11 uptake within the tumor compared with background liver
900 activity. (C) Corresponding arterial-phase (15 seconds) contrast-enhanced CT demonstrating
901 non-uniform contrast uptake in the tumor. Kidneys (K) demonstrate increased uptake due to
902 urinary excretion of the tracer. The high uptake in the spleen (S) relative to liver contrasts with
903 the relatively low splenic uptake reported in human patients. (D) three-dimensional maximum
904 intensity projection PET and (E) fused coronal PET and delayed phase contrast-enhanced CT
905 images demonstrating high peripheral tracer uptake in the hepatic tumor (white arrows) relative
906 to normal liver (black arrows), increased uptake in the kidneys (K) and pancreas (P), and no
907 uptake in spleen (S). (F) Corresponding arterial-phase (20 seconds) contrast-enhanced CT

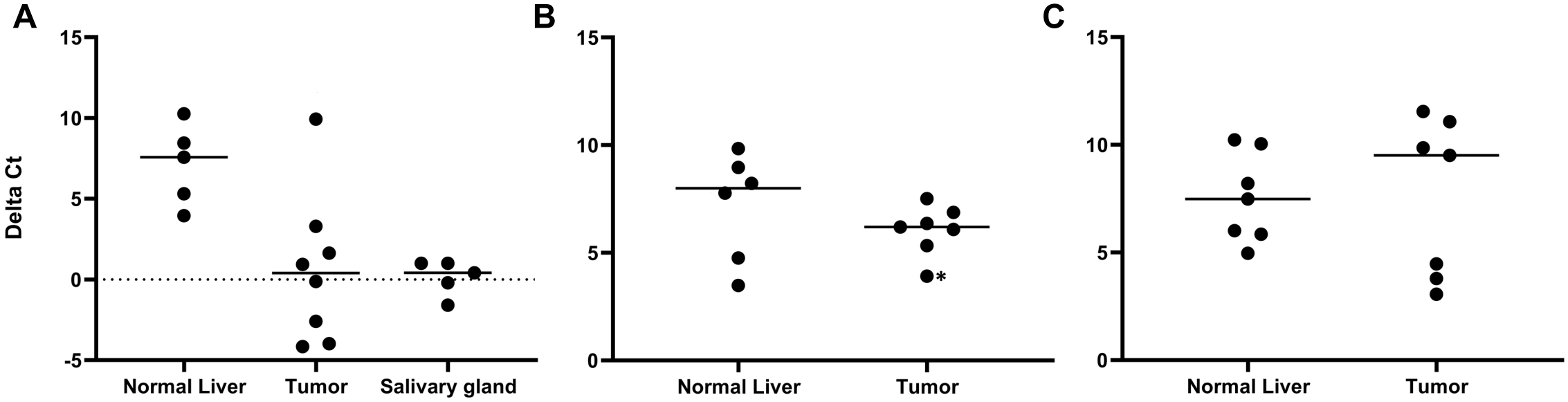
908 demonstrating peripheral contrast uptake in the tumor. PET signal is displayed on a 0–5 scale; R
909 denotes the right side and L the left side.
910
911 **Figure 3.** Physiological [^{68}Ga]Ga-PSMA-11 uptake in woodchuck salivary glands and testicles.
912 Fused axial PET/CT images of the head (A) and pelvic (B) regions of an adult woodchuck with
913 WHV-induced hepatocellular carcinoma, acquired 1 h after [^{68}Ga]Ga-PSMA-11 injection,
914 showing physiological uptake in salivary glands (A) and testicles (B). (A) White arrows indicate
915 the temporal salivary glands, and black arrows indicate the mandibular salivary glands. (B)
916 White arrows indicate testicles. PET signal is displayed on a 0–5 scale (left); R denotes the right
917 side.
918
919 **Figure 4.** Anterior gamma-camera image of a female woodchuck following [^{177}Lu]Lu-PSMA-
920 617 administration. The image was acquired 80 minutes following IV administration of 729
921 MBq [^{177}Lu]Lu-PSMA-617. White arrows indicate the mandibular salivary glands, black arrow
922 denotes hepatocellular carcinoma, and the grey arrow indicates liver uptake. Kidneys (K) and
923 bladder (B) are also labeled. Radiotracer uptake was present in the mandibular salivary glands at
924 the 60-minute timepoint and all subsequent imaging timepoints.
925
926 **Figure 5.** Histopathology of hepatocellular carcinoma (HCC) and regional lymph node in a
927 woodchuck. (A) Hematoxylin and eosin (H&E)-stained section of HCC (20x) demonstrating
928 prominent vacuolar change (grey arrow), areas of fibrosis (white arrow), and marked
929 inflammatory infiltrates (black arrow). (B) H&E-stained section of HCC (40x) showing
930 multinucleated cytomegalic cells (black arrows) located within sinusoidal spaces. (C) H&E-

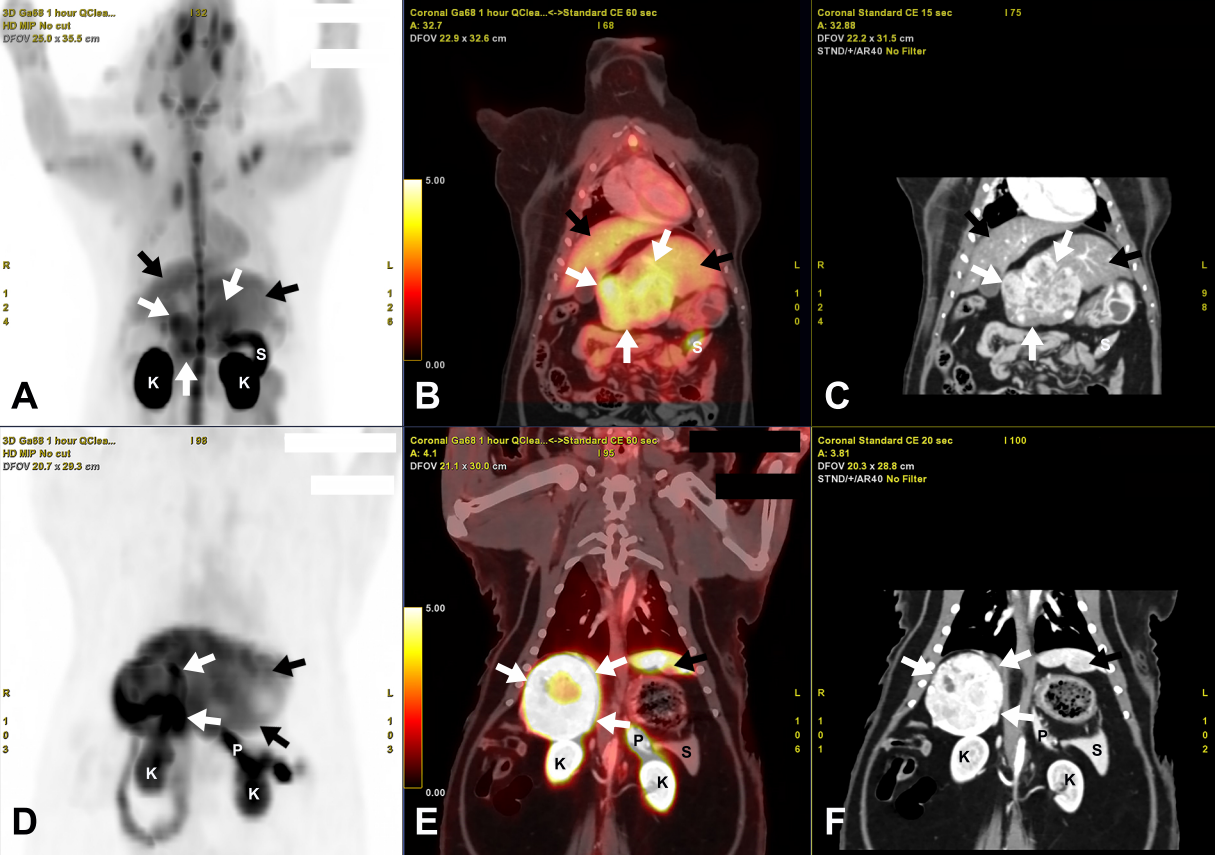
stained section of a hepatic lymph node (40x) from a woodchuck with regional metastatic HCC, containing multinucleated cytomegalic cells (black arrows).

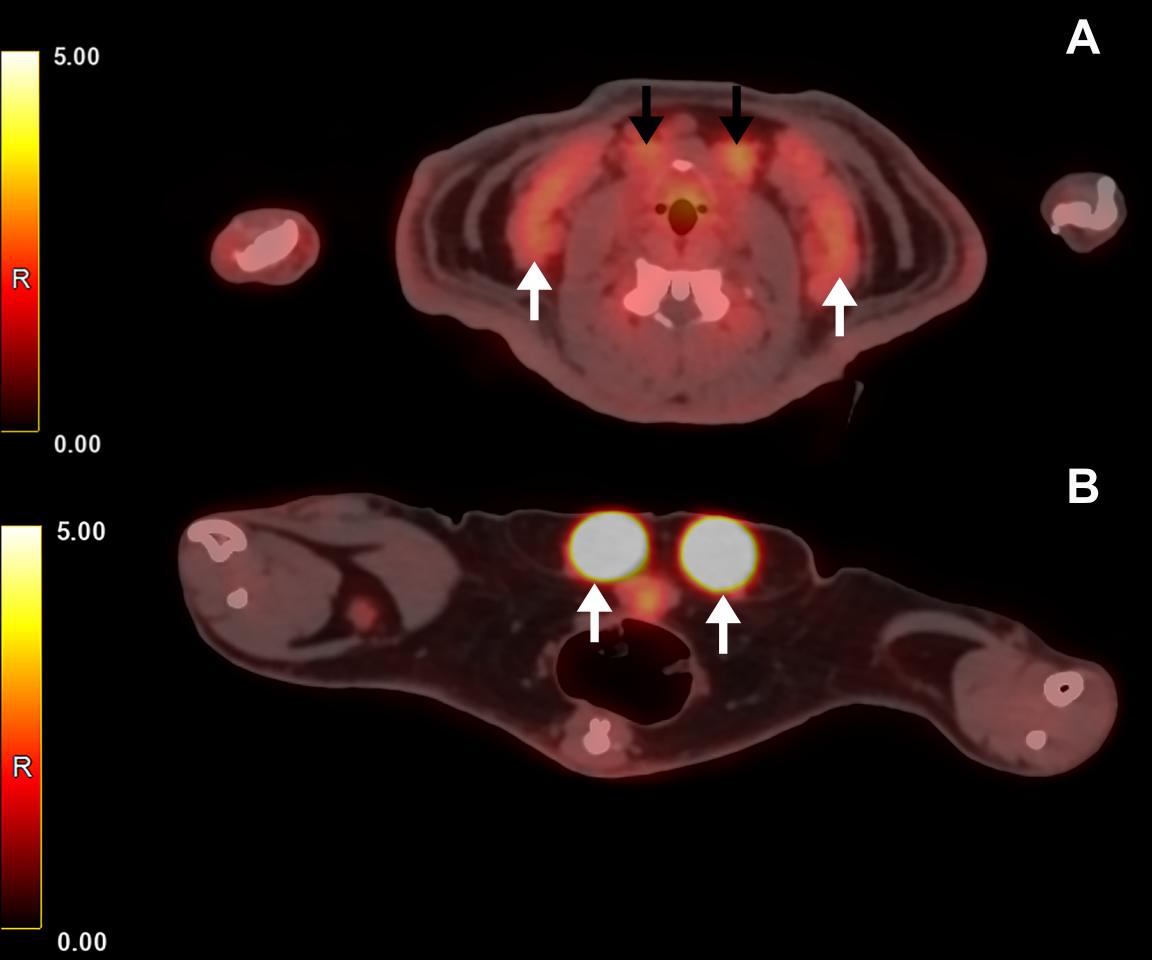
Figure 6. Immunohistochemical characterization of PSMA (A-C), SSTR2 (D), and SSTR5 (E, F) expression in woodchuck tissues. Brown chromogen indicates positive staining in all panels. (A) Membranous microvascular staining in hepatocellular carcinoma (HCC) (20x) using a mouse monoclonal antibody against human PSMA. (B) Cytoplasmic and membranous staining in mandibular salivary gland (40x) using anti-human PSMA antibody. (C) Strong cytoplasmic and membranous staining in testicular tissue (20x) using anti-human PSMA antibody. (D) Cytoplasmic staining in HCC (40x) using a rabbit monoclonal antibody against human SSTR2 in a tumor demonstrating uptake on [^{68}Ga]Ga-DOTATOC PET imaging. (E) Cytoplasmic staining in HCC (40x) using a rabbit polyclonal antibody against human SSTR5 in the same tumor. (F) Cytoplasmic staining in pancreatic tissue (40x) using a rabbit polyclonal antibody against human SSTR5.

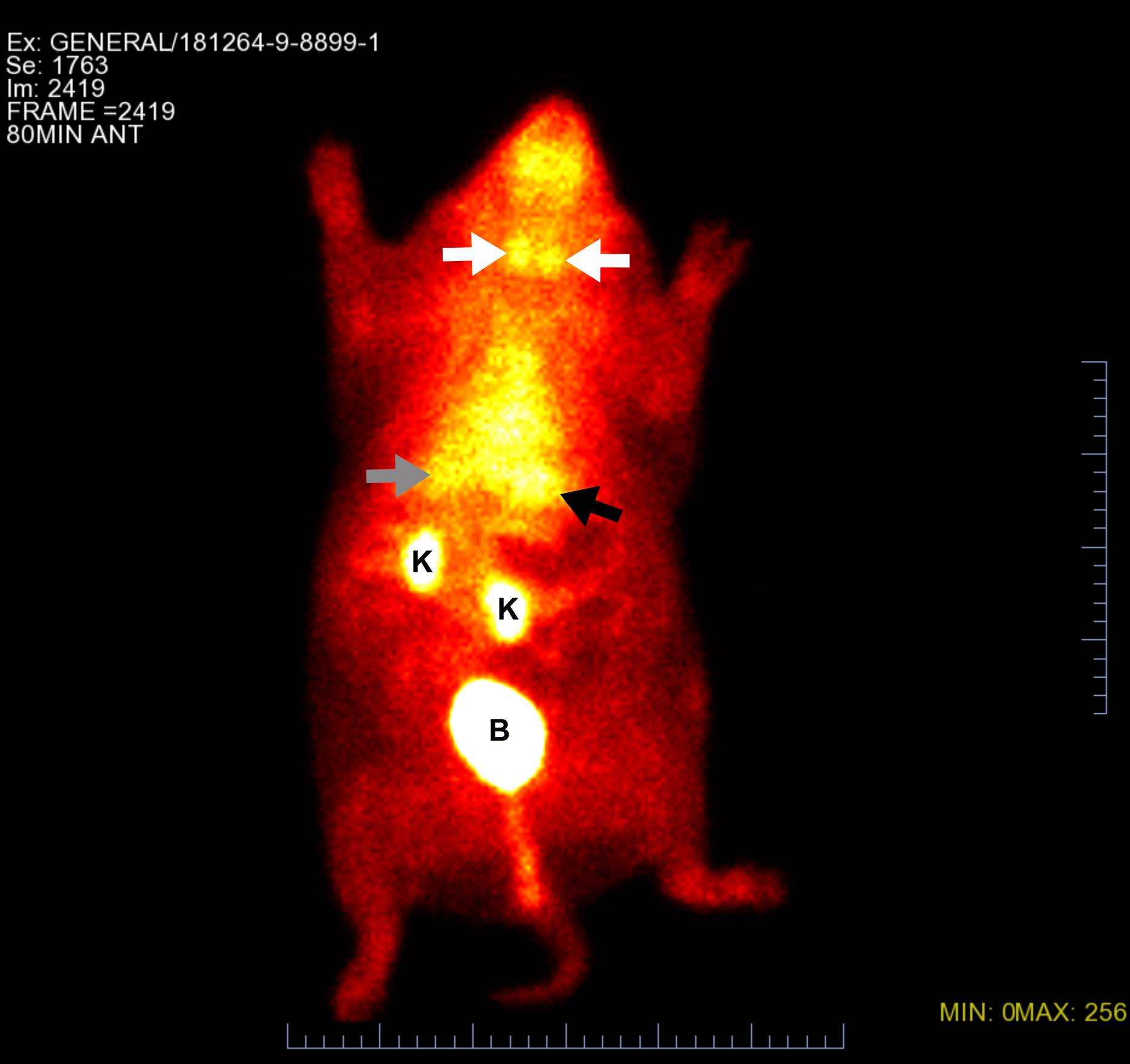
Figure 7. Immunohistochemical staining intensity across woodchuck tissues for two antibodies against human PSMA. Two mouse monoclonal antibodies were used (antibody 1: 1:25 dilution, Cat. No. PSMA-L, clone 1D6; Leica Biosystems; antibody 2: 1:100 dilution, Cat. No. MABN2300, clone 3F11; MilliporeSigma Canada). Heat maps show the proportion of samples exhibiting weak, moderate or strong staining intensity (no sample was scored as absent). Sample sizes for each tissue are indicated in parentheses. Color intensity represents the percentage of samples within each staining category, with darker shades indicating a higher proportion of

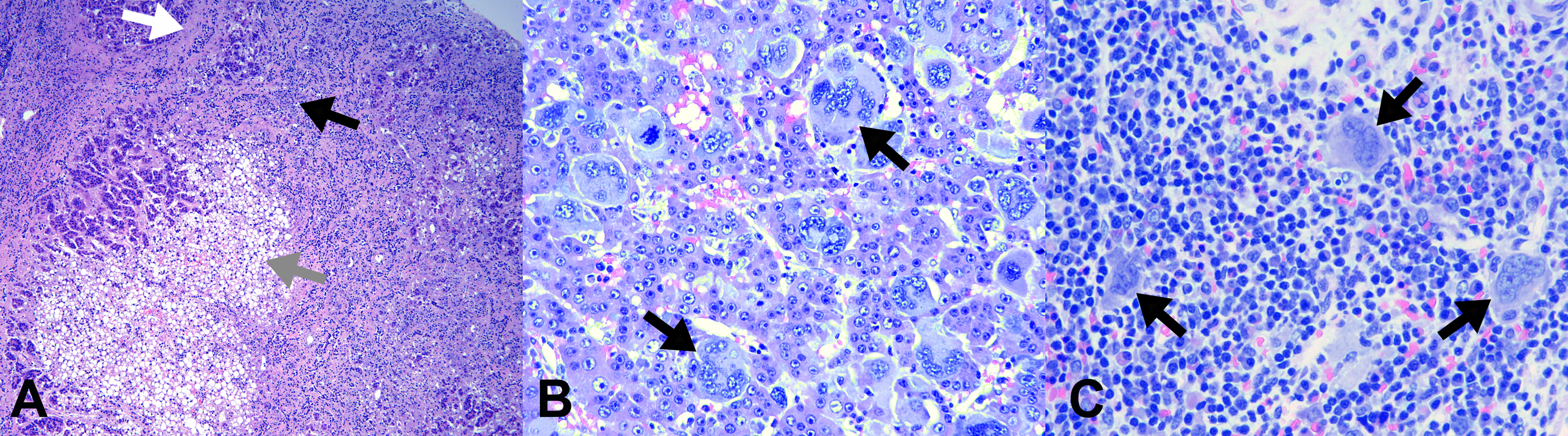
953 samples. Staining intensity was assessed semi-quantitatively based on signal intensity and
954 distribution within tissue sections. Salivary gland samples were from the mandibular glands.

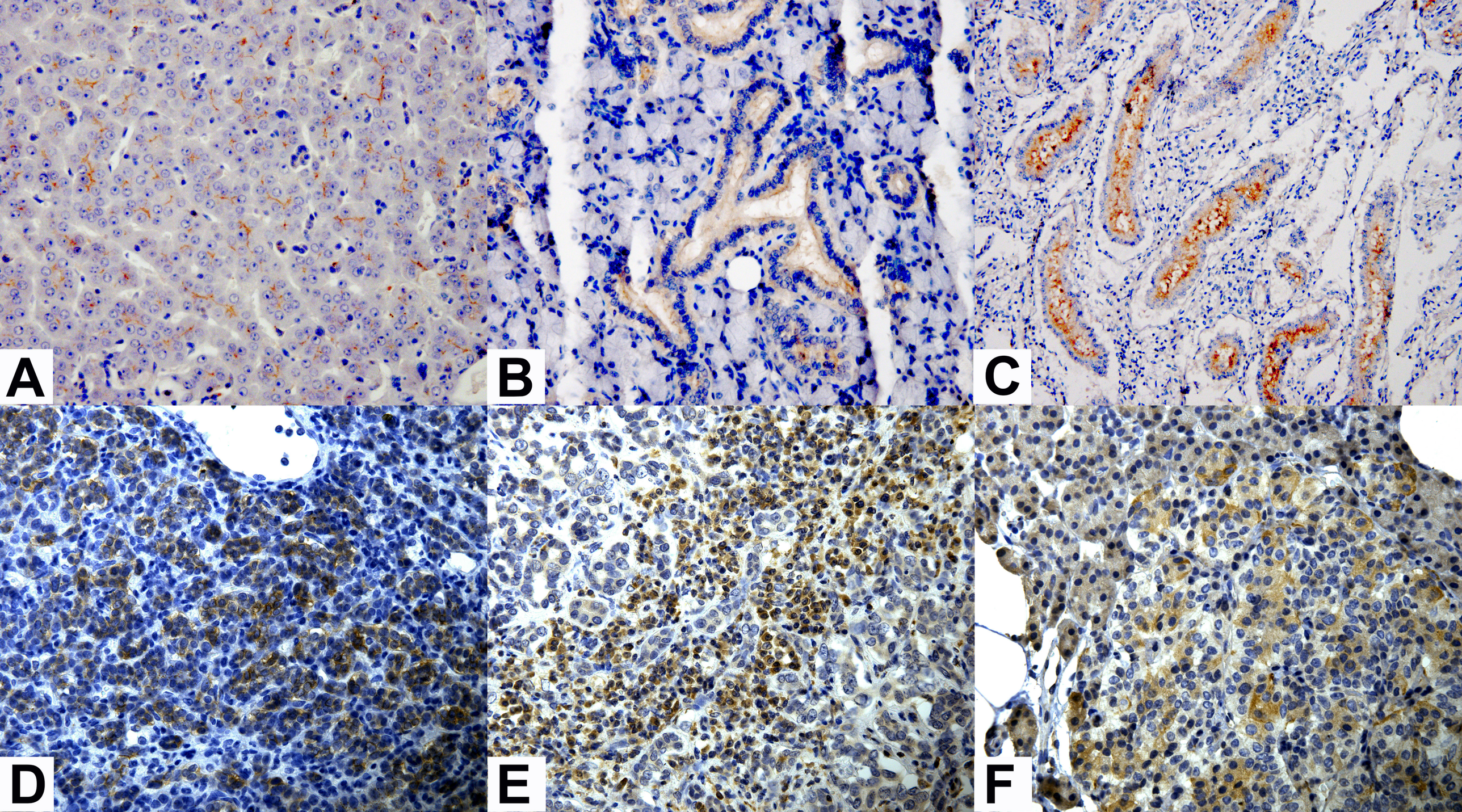

A
B
C
Delta Ct
15
10
5
0
-5
Normal Liver
Tumor
Salivary gland
*

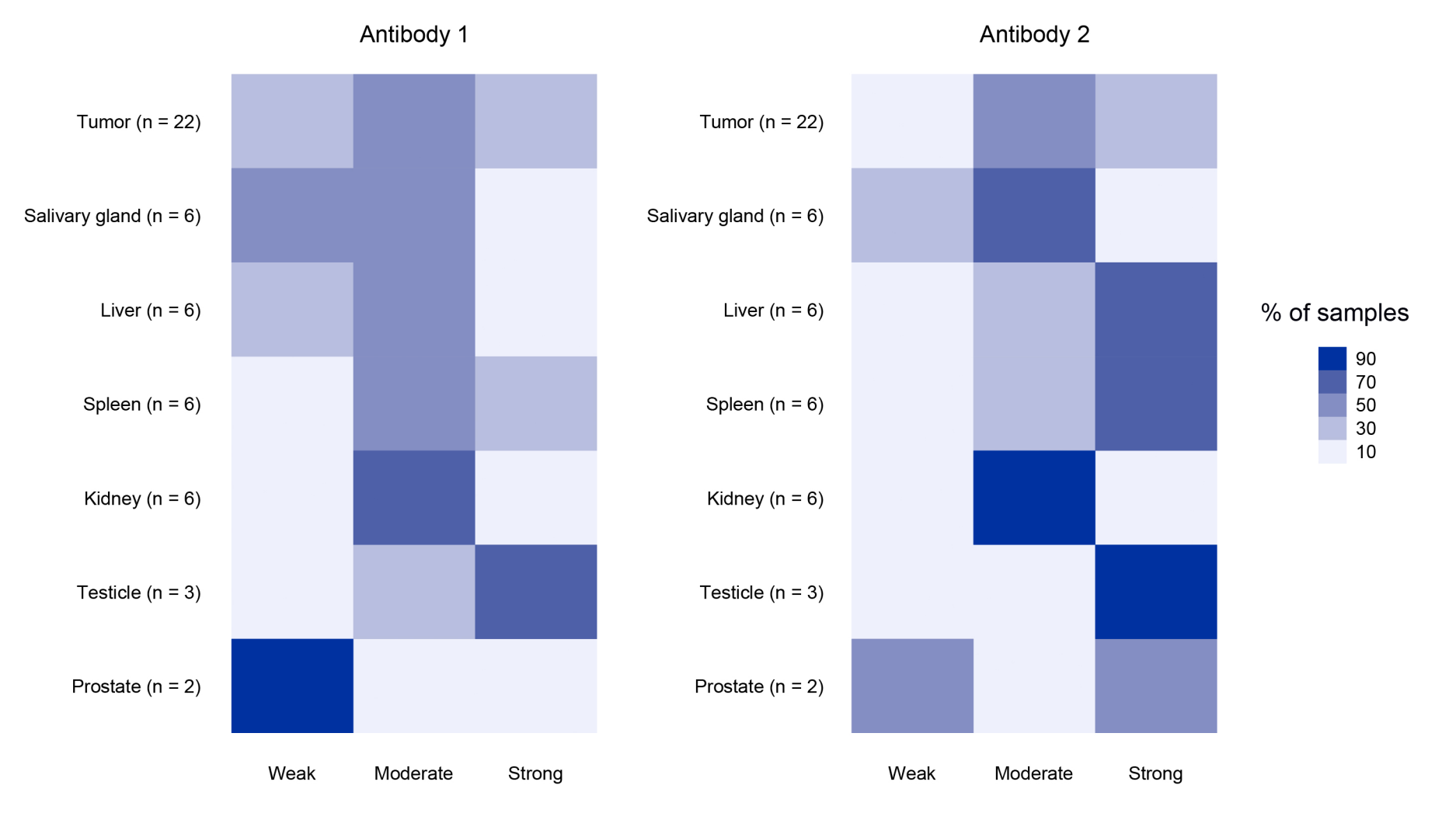

3D Ga68 1 hour QClea...
I 92
HD MIP No cut
DFOV 25.0 x 35.5 cm
R
L
1
2
4
S
K
K
A
Coronal Ga68 1 hour QClea...<->Standard CE 60 sec
A: 32.7
I 68
DFOV 22.9 x 32.6 cm
5.00
0.00
L
1
0
0
S
B
Coronal Standard CE 15 sec
I 75
A: 32.88
DFOV 22.2 x 31.5 cm
STND/+/AR40 No Filter
R
L
1
0
2
4
9
8
S
C
3D Ga68 1 hour QClea...
I 98
HD MIP No cut
DFOV 20.7 x 29.3 cm
R
L
1
0
3
K
P
K
D
Coronal Ga68 1 hour QClea...<->Standard CE 60 sec
A: 4.1
I 95
DFOV 21.1 x 30.0 cm
5.00
0.00
L
1
0
6
K
P
S
K
E
Coronal Standard CE 20 sec
I 100
A: 3.81
DFOV 20.3 x 28.8 cm
STND/+/AR40 No Filter
R
L
1
0
1
2
K
P
S
K
F


A
5.00
R
0.00
B
5.00
R
0.00


Ex: GENERAL/181264-9-8899-1
Se: 1763
Im: 2419
FRAME =2419
80MIN ANT
K
K
B
MIN: 0MAX: 256


A
B
C


A
B
C
D
E
F


Antibody 1
Antibody 2
Tumor (n = 22)
Salivary gland (n = 6)
Liver (n = 6)
Spleen (n = 6)
Kidney (n = 6)
Testicle (n = 3)
Prostate (n = 2)
Weak
Moderate
Strong
% of samples
90
70
50
30
10

Supplementary Files

This is a list of supplementary files associated with this preprint. Click to download.

- AdditionalFile1.xlsx